







# Enhanced Field Emission from Argon Plasma-Treated Ultra-sharp $\alpha$ -Fe<sub>2</sub>O<sub>3</sub> Nanorakes

Z. Zheng , Liao , Yan , X. Zhang   
Hao Gong , X. Shen , Yu

Received: 6 February 2009 / Accepted: 26 May 2009 / Published online: 12 June 2009  
to the authors 2009

**Abstract** Hematite nanorakes have been synthesized by a simple heat oxide method and further treated by Argon plasma. The effects of Argon plasma on the morphology and crystal structures of nanorakes were investigated.

Significant enhancement of field-induced electron emission from the plasma-treated nanorakes was observed. Transmission electron microscopy investigation shows that the plasma treatment effectively removes amorphous coating and creates plenty of sub-tips at the surface of nanorakes, which are believed to contribute the enhancement of emission. This work suggests that plasma treatment technique could be a direct means to improve emission properties of nanostructures.

**Keywords** Field emission · Metal oxide · Plasma treated

## Introduction

One-dimensional (1-D) and quasi-1-D nanostructures, due to their high crystal quality, large aspect ratio and sharp tips are well known as promising candidates for applications related to cold cathode, field emission of electrons [1]. Field emission is also called Fowler-Nordheim tunneling [2] is a form of quantum tunneling in which

electrons pass through a barrier in the presence of a high electric field. This phenomenon is highly dependent on both the structural properties of materials and the shape of particular cathode.

Practically, high current density and low turn-on field are the most desirable properties for electron emitters. For given materials, field-emission properties are mainly dependent on the morphologies like dimension and apex geometry of 1-D and quasi-1-D nanostructures. To improve the field-emission properties of nanostructures, several methods were employed before and after the synthesis process, for example, increasing the carrier concentration by a heavily ion doping method [3] or modifying the apex geometry by gas plasma treatment [4].

Recently, experiments have shown that emission current density of carbon nanotubes could be effectively enhanced by plasma treatments, which are capable of functionalizing and modifying the surface structure of carbon nanotubes. In addition to carbon nanotubes, gas plasmas like H<sub>2</sub>, Ar [7],

CO<sub>2</sub>, and CF<sub>4</sub> [4] have also been adopted to modify other nanomaterials. The results demonstrate plasma treatment could be a simple and efficient method to improve the field-emission performance of nanostructures. Argon (Ar) plasma is one kind of clean and non-toxic gas plasmas, which can be widely used in research and industry field. However, the effect and mechanism of Ar plasma treatment for the field-emission properties of metal oxide nanostructures have rarely been addressed in the literature [8], although there are a plenty of publications in the field of carbon nanotubes [9, 10].

Hematite ( $\alpha$ -Fe<sub>2</sub>O<sub>3</sub>) is one of the most important magnetic materials and shows numerous potential applications, such as the active component of gas sensors [11], photocatalyst [12], Lithium ion battery [13], and enzyme immunoassay [14]. The  $\alpha$ -Fe<sub>2</sub>O<sub>3</sub> nanorakes grown atomic force microscope (AFM) tips [15] exhibit promising electron field

Z. Zheng · L. Liao · B. Yan · Z. X. Shen · T. Yu (✉)  
Division of Physics and Applied Physics, School of Physical and Mathematical Sciences, Nanyang Technological University,  
Singapore 637371, Singapore  
e-mail: yuting@ntu.edu.sg

J. X. Zhang · H. Gong  
Department of Materials Science and Engineering, National  
University of Singapore, Blk E3A, 9 Engineering Drive 1,  
117576 Singapore, Singapore

emission properties at first time. Our previous works have demonstrated that  $\alpha$ - $\text{Fe}_2\text{O}_3$  nanoribbons could be one of the promising candidates as future field-emission electro sources and displays (FEDs) [6]. In this work, we report the effects of Ar plasma treatment on the crystal structure and morphology of  $\alpha$ - $\text{Fe}_2\text{O}_3$  nanoribbons. The field-emission properties of the plasma-treated  $\alpha$ - $\text{Fe}_2\text{O}_3$  nanoribbon film were also investigated.

## Experiment Part

The  $\alpha$ - $\text{Fe}_2\text{O}_3$  nanoribbons were synthesized by heating Fe foil on a conventional hot plate at atmosphere environment, as described in our previous work [6, 17]. The growth temperature and duration were fixed at 260 and 15 h respectively. The plasma treatment was conducted by plasma etching system (March PX-250) under the following conditions: radio-frequency (RF) frequency of 13.56 MHz, flow rate of 20 sccm, operating pressure of 0.2 Torr, RF power of 100 W, and process duration of 10 min.

The morphologies of the as-prepared and plasma-treated products were examined by scanning electron microscope (SEM) (JEOL JSM-6700F) while the compositions of their top surface were characterized by X-ray diffraction (XRD) (Bruker D8 with  $\text{Cu K}\alpha$  irradiation) and micro-Raman spectroscopy (Witech CRM200,  $\lambda_{\text{laser}} = 532 \text{ nm}$ ). The transmission electron microscopy (TEM) (JEOL JEM 2010F, 200 kV) observation shows the detailed morphology and crystal structure of the ultra-sharp nanoribbons. Field-emission measurements were carried out in a vacuum chamber with a pressure of  $3.8 \times 10^{-7}$  Torr at room temperature under a two-parallel-plate configuration. Details of the measurement system and procedure were reported previously [18]. The distance between electrodes was kept at 100  $\mu\text{m}$  with a measured emission area of 280  $\text{mm}^2$ .

## Results and Discussion

Figure 1 shows the SEM image of the as-prepared sample obtained. The random aligned nanoribbons synthesized at this temperature are about 20 nm at the bases, 5 nm at the tips, and 1  $\mu\text{m}$  in length in general. From the high magnification SEM image inset of Fig. 1, it can be clearly seen that there are semispherical tips at the thin ends of the nanoribbons.

Figure 2a illustrates the XRD patterns of the as-prepared sample and the plasma-treated sample. The rhombohedral  $\alpha$ - $\text{Fe}_2\text{O}_3$  with lattice constants  $a = 5.035 \text{ \AA}$  and  $c = 13.749 \text{ \AA}$  are readily confirmed from the XRD pattern universal narrowing of peak width for the plasma-treated samples, which exhibits that the overall crystal quality of the nanoribbons might be improved by the plasma treatment.

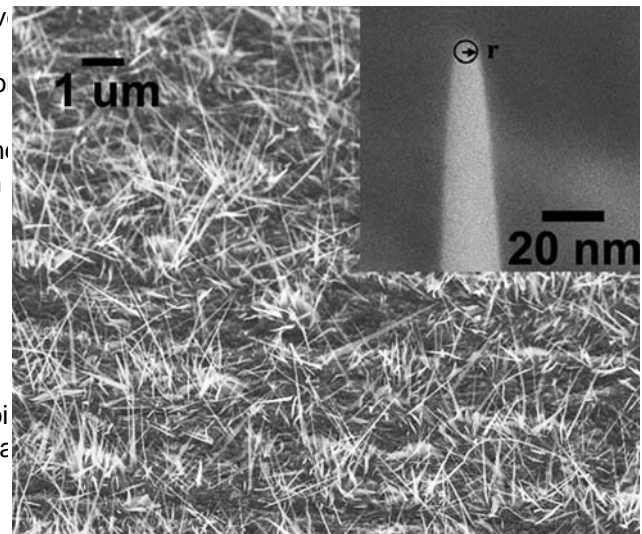


Fig. 1 SEM images of the top surfaces of Fe foils heated for 15 h at 260 C. Inset shows the high-magnification SEM images of the nanoribbon tip and the circle shows the radius of curvature at the nanoribbon tip

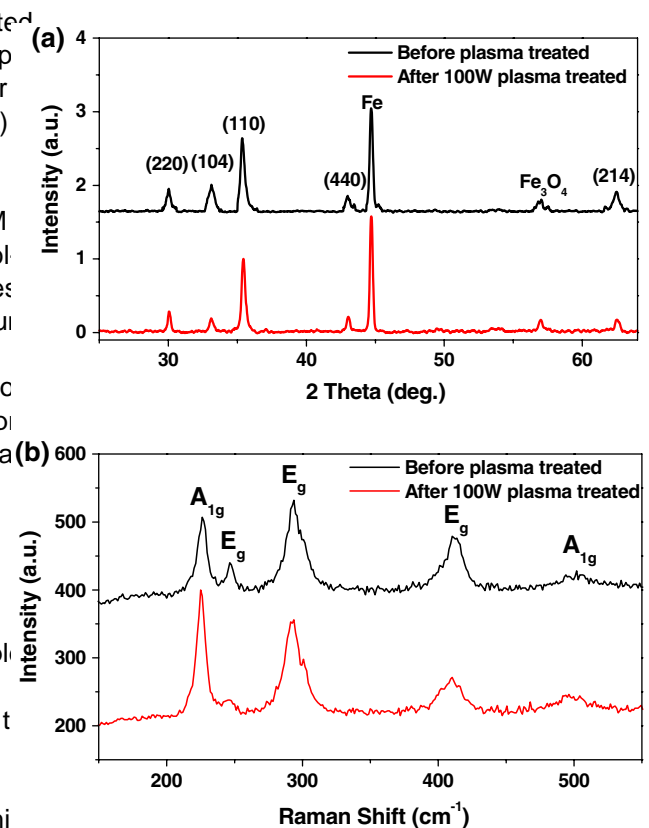


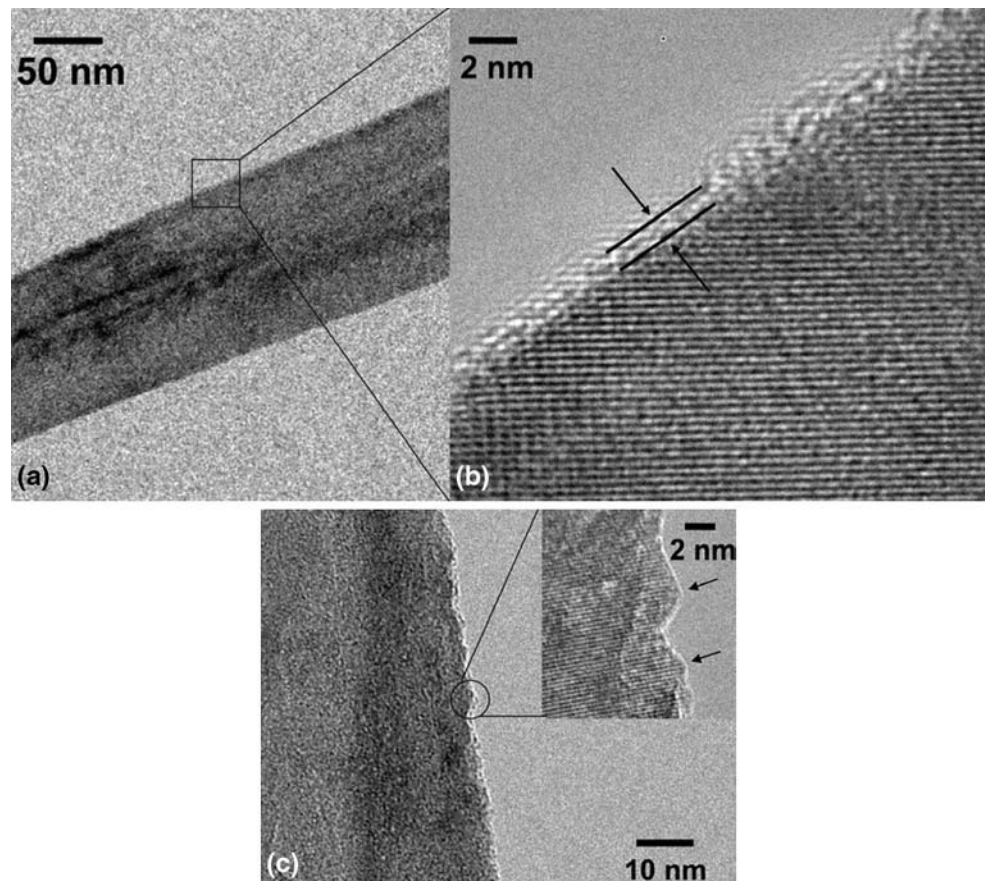
Fig. 2 a XRD patterns and b Raman spectra of the as-prepared sample and Ar plasma-treated samples

The Raman spectra of these PIm samples are shown in Fig. 2b. In the range of 1500–550  $\text{cm}^{-1}$ , there are five peaks located at 225, 245, 291, 408, and 499  $\text{cm}^{-1}$  corresponding to the  $\alpha\text{-Fe}_2\text{O}_3$  phase [20], namely two  $A_{1g}$  modes (225 and 499  $\text{cm}^{-1}$ ) and three  $E_g$  modes (245, 291, and 408  $\text{cm}^{-1}$ ). The same as the XRD pattern, no new peaks appear in the Raman spectrum of the plasma-treated sample, which indicates that the Ar plasma treatment did not introduce any new phase into the original  $\alpha\text{-Fe}_2\text{O}_3$  nanoßakes. After the Ar plasma treatment, some of the peaks (245, 291, and 408  $\text{cm}^{-1}$ ) become relatively weaker, which may be due to the surface defects on the nanoßakes coming from the plasma treatment. However, the peak position did not shift at all after plasma treatment demonstrating that this kind of perfection in  $\alpha\text{-Fe}_2\text{O}_3$  nanoßakes significantly. The XRD patterns and Raman spectra can be only used to illustrate the influence of the plasma treatment on total PIm samples. The detailed effects of the plasma treatment on  $\alpha\text{-Fe}_2\text{O}_3$  nanoßakes surface structures need to be further confirmed by other characterization methods.

To further reveal the influence of the Ar plasma treatment on the structure of the surface and interior of the nanoßakes, TEM was employed. Figure 3 displays

the representative TEM images of  $\alpha\text{-Fe}_2\text{O}_3$  nanoßakes before and after Ar plasma treatment for 10 min. As can be seen in the high-resolution TEM (HRTEM) image (Fig. 4b) of the region highlighted by a square in Fig. 3a, a very thin amorphous layer covers the surface of the as-grown nanoßakes, which is shown between two solid black lines. A typical low-magnification TEM image of the plasma-treated nanoßakes is shown in Fig. 3c. It is obvious that the amorphous layer was totally removed by Ar plasma and the nanoßakes became atomic scale clean. More importantly, plenty of surface protrusions as indicated by the arrows were formed by plasma treatment (Inset of Fig. 4c). The extension of the crystal lattice readily demonstrates that such protrusions of 1–3 nm in size are epitaxially connected with the original round tip body. Considering the above-mentioned XRD, Raman, and TEM results, the main effect of Ar plasma treatment in this work is removing the amorphous layer and creating nano protrusions. The projected structure can be seen through a bright-field TEM image of one  $\alpha\text{-Fe}_2\text{O}_3$  nanoßake (Fig. 4a). The corresponding dark-field TEM further confirms the existence of the protrusions on the surface of plasma-treated nanoßakes (Fig. 4b).

Fig. 3 a TEM image of the  $\alpha\text{-Fe}_2\text{O}_3$  nanoßake before plasma treatment, b High-resolution TEM image of a, c TEM image of the  $\alpha\text{-Fe}_2\text{O}_3$  nanoßake after plasma treatment. Inset of c shows the high-resolution TEM image of the highlighted part



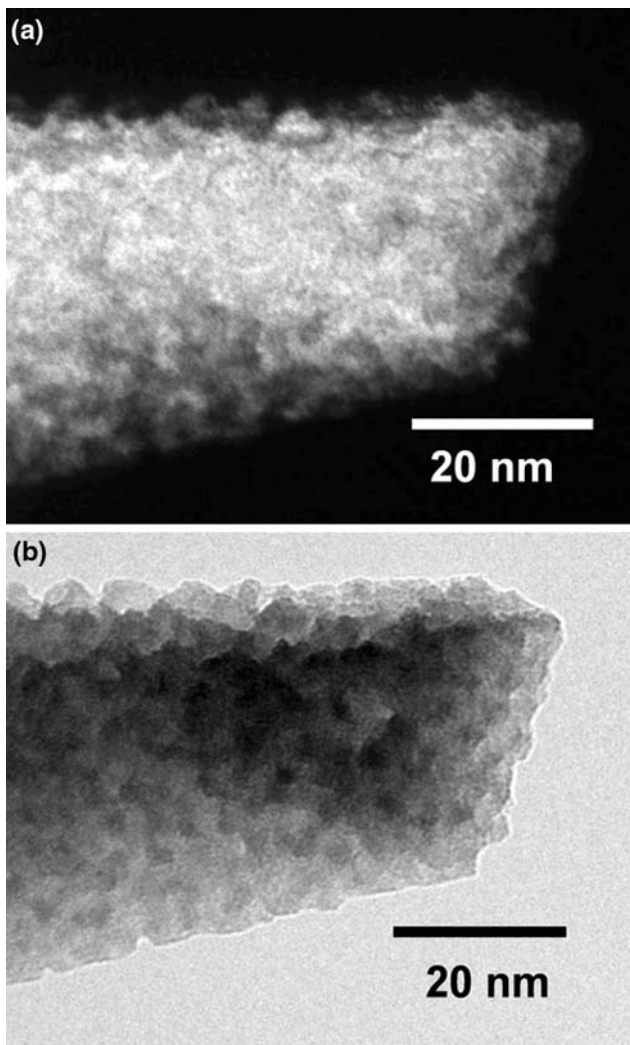


Fig. 4 a Dark-field and b bright-field TEM images of the tip of the  $\alpha\text{-Fe}_2\text{O}_3$  nano-sake after plasma treatment

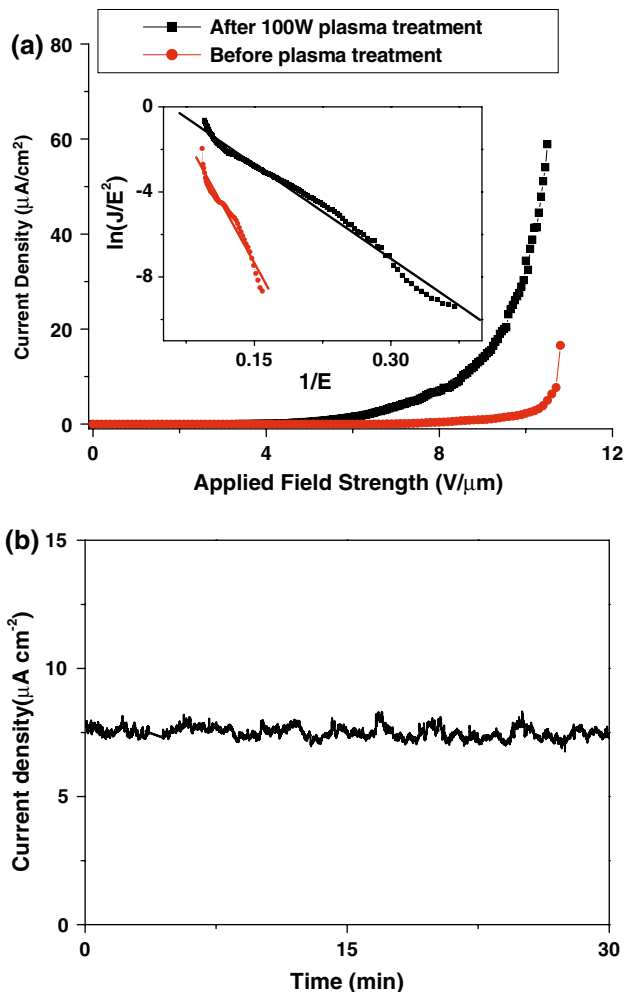


Fig. 5 a Typical field-emission current density vs. Applied field strength curves of the  $\alpha\text{-Fe}_2\text{O}_3$  nano-sakes PLMs before and after 100 W Ar plasma treatment. Inset shows the  $F-N$  plots ( $\ln(J/E^2)$  vs.  $1/E$ ) accordingly, which exhibits a good linear dependence (solid line is the fitting result). b Long-term stability measurement of field-emission property of nano-sake PLMs after Ar plasma treatment

treatment. The as-grown and plasma-treated nano-sakes exhibit significantly different emission behaviors. Detailed measurements reveal that the electron emission performance of the plasma-treated samples has been dramatically improved. For example, the maximum current density (under the field of  $11 \text{ V}/\mu\text{m}^{-1}$ ) has been increased from the original  $16 \text{ D}60 \mu\text{A cm}^{-2}$ . At the same time, the turn-on field has been reduced from  $10$  to  $8 \text{ V}/\mu\text{m}^{-1}$  after 10 min exposure to Ar plasma. The exponential dependence between the emission current and the applied field, plotted by the  $\ln(J/E^2) - 1/E$  relationship (inset of Fig. 5a) were found for both as-grown and plasma-treated samples, indicating that the field emission from  $\alpha\text{-Fe}_2\text{O}_3$  nano-sake PLMs follow the Fowler-Nordheim (FN) relationship [21]. The dots are experimental data and the solid lines are the fitted curves in accordance with the simplified Fowler-Nordheim equation [21]:

$$J = \frac{A(\beta E)^2}{\phi} \exp\left[-\frac{B\phi^{3/2}}{\beta E}\right] \tag{1}$$

where  $J$  is the current density,  $E$  is the local field strength;  $\phi$  is the work function, for electron emission which is estimated to be  $5.4 \text{ eV}$  [22] for  $\alpha\text{-Fe}_2\text{O}_3$ ;  $A$  and  $B$  are constants with the value of  $1.54 \times 10^{-6} \text{ A V}^{-2} \text{ eV}$  and  $6.83 \times 10^7 \text{ V cm}^{-1} \text{ eV}^{-3/2}$  [21] respectively. For nanostructures, the local field is usually much stronger than the applied field  $E_{\text{app}}$ , and modified by a field enhancement factor  $\beta$  as defined by:

$$E = \beta E_{\text{app}} = \beta \frac{V}{d} \tag{2}$$

$\beta$  is a parameter depending on the aspect ratio of the nanostructures, crystal structures, and the density of the

emitting points;  $d$  is the average spacing between the electrodes ( $d = 100 \mu\text{m}$  in this work) and  $V$  is the applied voltage.  $\beta$  was obtained to be 1,131 from the linear fitting of the FDN curve at turn-on area while that of Ar plasma-treated nanostructures was 3,218. This enhanced factor is higher or comparable to many other nanostructures, such as the AlN nanoneedles ( $\beta = 748$ ) [23] and the ZnO nanopins [3] ( $\beta = 2317$ ).

The field-emission stability of the plasma-treated  $\text{Fe}_2\text{O}_3$  nanostructure films was investigated and the typical result is shown in Fig. 5b. The total emission current was monitored over 30 min under an applied macroscopic field of  $9 \text{ V } \mu\text{m}^{-1}$  and an emitter-anode gap of  $100 \mu\text{m}$ . At an emission current density of  $7 \mu\text{A cm}^{-2}$ , the fluctuations were  $<5\%$  and no degradations were observed. Comparing with our previous results [7], it is believed that the Ar plasma treatment will not only improve the current density but also extend the stability of the field-emission current. These results reveal the possibility of Ar plasma treatment to improve the field-emission performance.

Based on the morphological and crystal structural investigations, the enhancement of field emission by Ar plasma treatment could be elucidated. First, the plasma etching process effectively removes the amorphous coating and cleans the nanostructures at atomic level. Second, ultra-sharp sub-tips of  $103 \text{ nm}$  could be created by the plasma treatment which can remarkably reduce the diameter of the emitter for increasing the field enhancement factor. At last, the density of emitters is significantly increased. All these effects could enhance the field enhancement factor and consequently improve the emission performance.

## Conclusion

In summary, the effects of Argon plasmas on the morphology and crystal structures of  $\text{Fe}_2\text{O}_3$  nanostructures were investigated. Our results successfully demonstrate that the plasma treatment could effectively clean the nanostructures, create plenty of ultra-sharp sub-tips and consequently significantly enhance the electron emission from plasma-treated nanostructures. The high current density and low turn-on field promise a potential for plasma-treated  $\text{Fe}_2\text{O}_3$  nanostructures as electron emitter. This work also demonstrates the plasma etching process might be a facile and efficient technique for improving electron emission of nanostructures.

1. Y. Xia, P. Yang, Y. Sun, Y. Wu, B. Mayers, B. Gates, Y. Yin, F. Kim, H. Yan, *Adv. Mater.* 15, 353 (2003). doi:10.1002/adma.200390087
2. Y. Khliil, K. Kassmi, L. Roubi, R. Maimouni, M.J. Condens. Matter. 3, 53 (2000)
3. C.X. Xu, X.W. Sun, B.J. Chen, *Appl. Phys. Lett.* 84, 1540 (2004). doi:10.1063/1.1651328
4. Y.W. Zhu, A.M. Moo, T. Yu, X.J. Xu, X.Y. Gao, Y.J. Liu, C.T. Lim, Z.X. Shen, C.K. Ong, A.T.S. Wee, J.T.L. Thong, C.H. Sow, *Chem. Phys. Lett.* 419, 458 (2006). doi:10.1016/j.cplett.2005.11.087
5. Y.W. Zhu, F.C. Cheong, T. Yu, X.J. Xu, C.T. Lim, J.T.L. Thong, Z.X. Shen, C.K. Ong, Y.J. Liu, A.T.S. Wee, C.H. Sow, *Carbon* 43, 395 (2005). doi:10.1016/j.carbon.2004.09.029
6. W.Y. Sung, W.J. Kim, S.M. Lee, H.Y. Lee, Y.H. Kim, K.H. Park, S. Lee, *Vacuum* 81, 851 (2007). doi:10.1016/j.vacuum.2006.10.002
7. J.W. Lee, H.N. Cho, S.R. Min, C.W. Chung, *Integr. Ferroelectr.* 90, 95 (2007). doi:10.1080/10584580701249371
8. S. Mathur, R. Ganesan, I. Grobelsek, H. Shen, T. Ruegamer, S. Barth, *Adv. Eng. Mater.* 9, 658 (2007). doi:10.1002/adem.200700086
9. S.C. Kung, K.C. Hwang, I.N. Lin, *Appl. Phys. Lett.* 80, 4819 (2002). doi:10.1063/1.1485315
10. K. Yu, Z. Zhu, M. Xu, Q. Li, W. Lu, *Chem. Phys. Lett.* 373, 109 (2003). doi:10.1016/S0009-2614(03)00541-4
11. J.S. Han, T. Bredow, D.E. Davey, A.B. Yu, D.E. Mulcahy, *Sens. Actuators B* 75, 18 (2001). doi:10.1016/S0925-4005(00)00688-2
12. S.N. Frank, A.J. Bard, *J. Phys. Chem.* 81, 1484 (1977). doi:10.1021/j100530a011
13. M.V. Reddy, T. Yu, C.H. Sow, Z.X. Shen, C.T. Lim, G.V. Subba Rao, B.V.R. Chowdari, *Adv. Funct. Mater.* 7, 2792 (2007). doi:10.1002/adfm.200601186
14. X.Y. Liu, X.B. Ding, Z.H. Zheng, Y.X. Peng, A.S.C. Chan, C.W. Yip, X.P. Long, *Polym. Int.* 52, 235 (2003). doi:10.1002/pi.1031
15. Y.W. Zhu, T. Yu, A.T.S. Wee, X. J. Xu, C.T. Lim, J.T.L. Thong, C.H. Sow, *Appl. Phys. Lett.* 87, 023103 (2005). doi:10.1063/1.1991978
16. Z. Zheng, Y.Z. Chen, Z.X. Shen, J. Ma, C.H. Sow, W. Huang, T. Yu, *Appl. Phys.* 89, 115 (2007). doi:10.1007/s00339-007-4180-9
17. T. Yu, Y.W. Zhu, X.J. Xu, K.S. Yeong, Z.X. Shen, P. Chen, C.T. Lim, J.T.L. Thong, C.H. Sow, *Small* 2, 80 (2006). doi:10.1002/sml.200500234
18. Y.W. Zhu, T. Yu, F.C. Cheong, X.J. Xu, C.T. Lim, V.B.C. Tan, J.T.L. Thong, C.H. Sow, *Nanotechnology* 16, 88 (2005). doi:10.1088/0957-4484/16/1/018
19. Joint Committee on Powder Diffraction Standards (JCPDS), Card No. 87-1166, hematite ( $\text{Fe}_2\text{O}_3$ )
20. I.R. Beattie, T.R. Gilson, *J. Chem. Soc.* 5A980 (1983)
21. R. Fowler, L.W. Nordheim, *Proc. R. Soc. Lond.* 119, 173 (1928). doi:10.1098/rspa.1928.0091
22. V.E. Hendrich, P.A. Cox, in *Surface science of metal oxides* (Cambridge University Press, Cambridge, UK, 1994)
23. Q. Zhao, J. Xu, X.Y. Xu, Z. Wang, D.P. Yang, *Appl. Phys. Lett.* 85, 5331 (2005). doi:10.1063/1.1825620